Geochemistry Geophysics Geosystems G3
AN ELECTRONIC JOURNAL OF THE EARTH SCIENCES
Published by AGU and the Geochemical Society

Article
Volume 11, Number 2
11 February 2010
Q02003, doi:10.1029/2009GC002879
ISSN: 1525-2027

Click Here for Full Article

Origin of apparent magnetic excursions in deep-sea sediments from Mendeleev-Alpha Ridge, Arctic Ocean

Chuang Xuan and James E. T. Channell
Department of Geological Sciences, University of Florida, 241 Williamson Hall, P.O. Box 112120, Gainesville, Florida 32611, USA (xuan2005@ufl.edu; jetc@ufl.edu)

[1] Arctic deep-sea sediments often record intervals of negative inclination of natural remanence that are tens of centimeters thick, implying magnetic excursions with durations of tens of thousand years that far exceed excursion durations estimated elsewhere, and the lack of tight age control usually provides excessive freedom in the labeling of Arctic excursions. Fortuitous variations in sedimentation rate have been invoked to explain the "amplified" excursions. Alternating field demagnetization of natural remanent magnetization (NRM) of sediment cores 08JPC, 10JPC, 11JPC, and 13JPC recovered by the Healy Oden Trans-Arctic Expedition in August 2005 (HOTRAX05) to the Mendeleev-Alpha Ridge yields apparent magnetic "excursions" in sediments deposited in the Brunhes Chron. Thermal demagnetization of the NRM, however, implies multiple magnetization components with negative inclination components usually "unblocked" below ~350°C. Analysis of isothermal remanent magnetization acquisition curves from magnetic extracts indicates two magnetic coercivity components superimposed on one another. Magnetic experiments conducted under high and low temperatures show features that are characteristic for (titano)magnetite and titanomaghemite. Presence of the two magnetic phases is further confirmed by elemental mapping on a scanning electron microscope equipped for X-ray energy dispersive spectroscopy (EDS) and by high-resolution X-ray diffraction (XRD). It is unlikely that anomalously thick intervals of negative inclination in these Brunhes-aged sediments are caused by unusual behavior of the magnetic field in the Arctic area. We therefore attribute low and negative NRM inclinations in these cores to partially self-reversed chemical remanent magnetizations, apparently carried by titanomaghemite and acquired during the oxidation of detrital (titano)magnetite grains. The high Ti contents and high oxidation states indicated by EDS and XRD data provide the conditions required for partial self-reversal by ionic reordering during diagenetic maghemitization, and this process appears to have affected all HOTRAX05 cores collected from the Mendeleev-Alpha Ridge.

Components: 7974 words, 10 figures, 2 tables.

Keywords: Arctic sediments; geomagnetic excursions; titanomaghemite; self-reversal.

Index Terms: 1533 Geomagnetism and Paleomagnetism: Remagnetization; 1513 Geomagnetism and Paleomagnetism: Geomagnetic excursions; 1540 Geomagnetism and Paleomagnetism: Rock and mineral magnetism.

Received 25 September 2009; **Revised** 30 November 2009; **Accepted** 14 December 2009; **Published** 11 February 2010.

Xuan, C., and J. E. T. Channell (2010), Origin of apparent magnetic excursions in deep-sea sediments from Mendeleev-Alpha Ridge, Arctic Ocean, *Geochem. Geophys. Geosyst.*, *11*, Q02003, doi:10.1029/2009GC002879.

1. Introduction

[2] The significance of the Arctic Ocean in understanding climate change has increased geological investigations in the Arctic since the 1960s. Limited biogenic productivity and high carbonate dissolution in the Arctic Ocean present a challenge for the construction of conventional biostratigraphy and isotopic stratigraphy. Magnetic stratigraphy has been important for providing age constraints for Arctic deep-sea sediments. Magnetic polarity patterns of sediment cores retrieved from the Northwind Ridge [e.g., *Poore et al.*, 1993; *Phillips and Grantz*, 1997], the Mendeleev-Alpha Ridge [e.g., *Steuerwald et al.*, 1968; *Hunkins et al.*, 1971; *Herman*, 1974; *Clark et al.*, 1980, 1984; *Witte and Kent*, 1988], and the Lomonosov Ridge [e.g., *Morris et al.*, 1985; *Spielhagen et al.*, 1997] often yielded sedimentation rates on the mm/kyr scale (see Figure 1 for location of these studied cores). In these studies, negative natural remanent magnetization (NRM) inclinations often occurred at a depth of 1–2 m below seafloor (mbsf), and were commonly interpreted as representing the Matuyama Chron. On the other hand, amino acid epimerization dating from a Mendeleev Ridge core suggested cm/kyr scale sedimentation rates [*Sejrup et al.*, 1984] inconsistent with earlier paleomagnetic data from the same core by *Herman* [1974]. The cm/kyr scale sedimentation rate in the Arctic Ocean was later supported by radiocarbon dating [e.g., *Darby et al.*, 1997], correlating manganese and color cycles to lower-latitude $\delta^{18}O$ records [*Jakobsson et al.*, 2000], and optically stimulated luminescence dating [*Jakobsson et al.*, 2003], as well as improved amino acid racemization ages [*Kaufman et al.*, 2008]. These methods were accompanied by poorly constrained biostratigraphic markers, such as the sporadic appearance of *E. huxleyi* indicative of the late Brunhes Chron. The present consensus is that cm/kyr scale sedimentation rates are evident throughout the Arctic Ocean [*Backman et al.*, 2004; *Spielhagen et al.*, 2004; *Polyak et al.*, 2009]. Accordingly, magnetic excursions of Brunhes age have often been invoked to explain the negative inclinations observed in the top several meters of the Arctic sediment sequences [e.g., *Løvlie et al.*, 1986; *Bleil*, 1987; *Nowaczyk and Baumann*, 1992; *Jakobsson et al.*, 2000; *Nowaczyk et al.*, 2001; *Spielhagen et al.*, 2004; *O'Regan et al.*, 2008], and magnetic excursion ages derived from outside the Arctic Ocean were often adopted as age control points for Arctic sediments. There are, however, obvious problems associated with the "excursion" interpretation. Due to the limited duration of magnetic excursions and smoothing effects of the magnetization lock-in process, even sediments with mean deposition rate >10 cm/kyr rarely preserve magnetic excursions [see *Roberts and Winklhofer*, 2004]. Negative inclination intervals in the Arctic sediments are often tens of centimeters thick implying excursion durations of >10 kyr [e.g., *Backman et al.*, 2008; *Channell and Xuan*, 2009]. Excursion durations estimated outside the Arctic region, however, are usually <5 kyr [see *Laj and Channell*, 2007], comparable with the ~3 kyr time scale for diffusive field changes in the Earth's solid inner core which provides a basis for the mechanistic distinction between excursions and long-lived reversals [*Gubbins*, 1999]. Fortuitous variations in sedimentation rates have to be invoked to explain the amplified "excursions," and the apparent "excursions" do not always correlate after stratigraphic alignment using sediment physical properties [e.g., *O'Regan et al.*, 2008]. *Jakobsson et al.* [2000] noted that, below their inferred Brunhes/Matuyama boundary in core 96/12-1pc from the Lomonosov Ridge, inclination patterns cannot be correlated to the geomagnetic polarity time scale without introducing major discontinuities in sedimentation rate.

[3] Magnetic studies on core 06JPC from the edge of the East Siberian shelf (Figure 1), along the Mendeleev-Alpha Ridge recovered by HOTRAX05 indicated that titanomagnetite and titanomaghemite are magnetic remanence carriers in the sediments [*Channell and Xuan*, 2009]. The authors proposed that negative inclinations in the sediments could have resulted from a partial self-reversed chemical remanent magnetization (CRM) acquired during the oxidation of primary titanomagnetite to titanomaghemite. In this paper, isothermal remanent magnetization (IRM) acquisition, high- and low-temperature rock magnetic experiments, scanning electron microscope (SEM), EDS, and high-resolution XRD observations were employed to investigate cores 08JPC, 10JPC, 11JPC, and 13JPC (Figure 1) further along the Mendeleev-Alpha Ridge of the Arctic Ocean in order to determine whether the results from core 06JPC are encountered along a traverse into the central Arctic ocean, further understand the origin of low and negative NRM inclinations that may be present in these sediments, and gauge the regional importance of

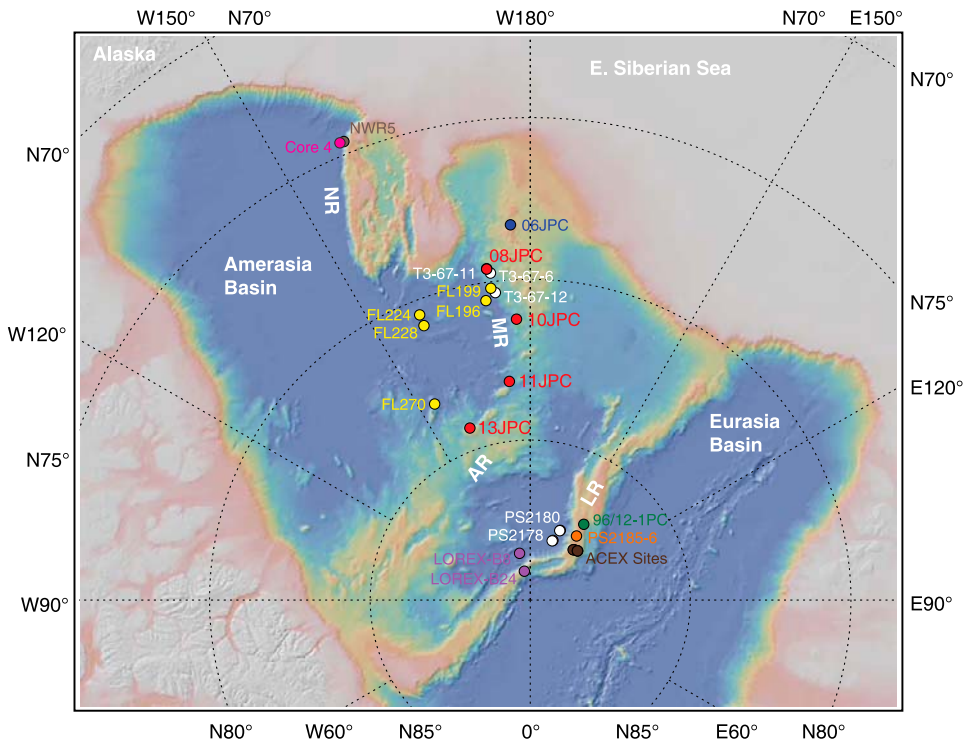

Figure 1. Locations of cores 08JPC, 10JPC, 11JPC, and 13JPC (red solid circles) retrieved by the HOTRAX05 in comparison with locations of previously studied cores. LR denotes Lomonosov Ridge, MR denotes Mendeleev Ridge, AR denotes Alpha Ridge, and NR denotes Northwind Ridge. Base map data are from international bathymetric chart of Arctic Ocean (IBCAO [*Jakobsson et al.*, 2008]). Map is processed using the GeoMapApp© software. References for previously studied cores listed on the map are as follows: NWR5, *Poore et al.* [1993]; core 4, *Phillips and Grantz* [1997]; T3-67-11, *Herman* [1974] and *Sejrup et al.* [1984]; T3-67-6 and T3-67-12, *Hunkins et al.* [1971] and *Witte and Kent* [1988]; FL224, *Steuerwald et al.* [1968] and *Clark et al.* [1980]; FL270 and FL228, *Clark et al.* [1980]; FL196 and FL199, *Clark et al.* [1984]; PS2180 and PS2178, *Nowaczyk et al.* [2001]; LOREX-B8 and LOREX-B24, *Morris et al.* [1985]; 96/12-1PC, *Jakobsson et al.* [2000]; PS2185-6, *Spielhagen et al.* [1997, 2004]; ACEX sites, *Backman et al.* [2008]; 06JPC, *Channell and Xuan* [2009].

the self-reversal mechanism proposed by *Channell and Xuan* [2009].

2. NRM Measurements

[4] U channel samples (typically $2 \times 2 \times 150$ cm^3) were collected from cores 08JPC, 10JPC, 11JPC, and 13JPC recovered by HOTRAX05 to the Mendeleev Ridge and Alpha Ridge (Figure 1 and Table 1). The sediments of these cores generally consist of dark brown to yellowish or grayish silts and silty clays with occasional coarse sand layers. The NRM of each u channel sample was measured at 1 cm intervals before demagnetization and after alternating field (AF) demagnetization at 10–14 steps in the 10–100 mT peak field range. For each step, samples from cores 08JPC, 10JPC, and 11JPC were measured after two separated demagnetization sequences for the X, Y and Z sample axes to monitor any spurious anhysteretic rema-

Table 1. Location, Length, Water Depth, and Age Model Information for Cores Studied in This Paper

Core	Location[a]	Latitude (°N)	Longitude (°W)	Length	Water Depth	Age Constraints[b]
HLY0503-08JPC	MR	79.593	172.502	11.88 m	2792 m	1–3
HLY0503-10JPC	MR	81.226	177.194	12.72 m	1865 m	3
HLY0503-11JPC	AR	83.144	177.194	10.19 m	2644 m	3
HLY0503-13JPC	AR	84.306	160.680	12.00 m	1400 m	3

[a] MR denotes Mendeleev Ridge, and AR denotes Alpha Ridge.
[b] References are as follows: 1, *Kaufman et al.* [2008]; 2, *Adler et al.* [2009]; 3, *Polyak et al.* [2009].

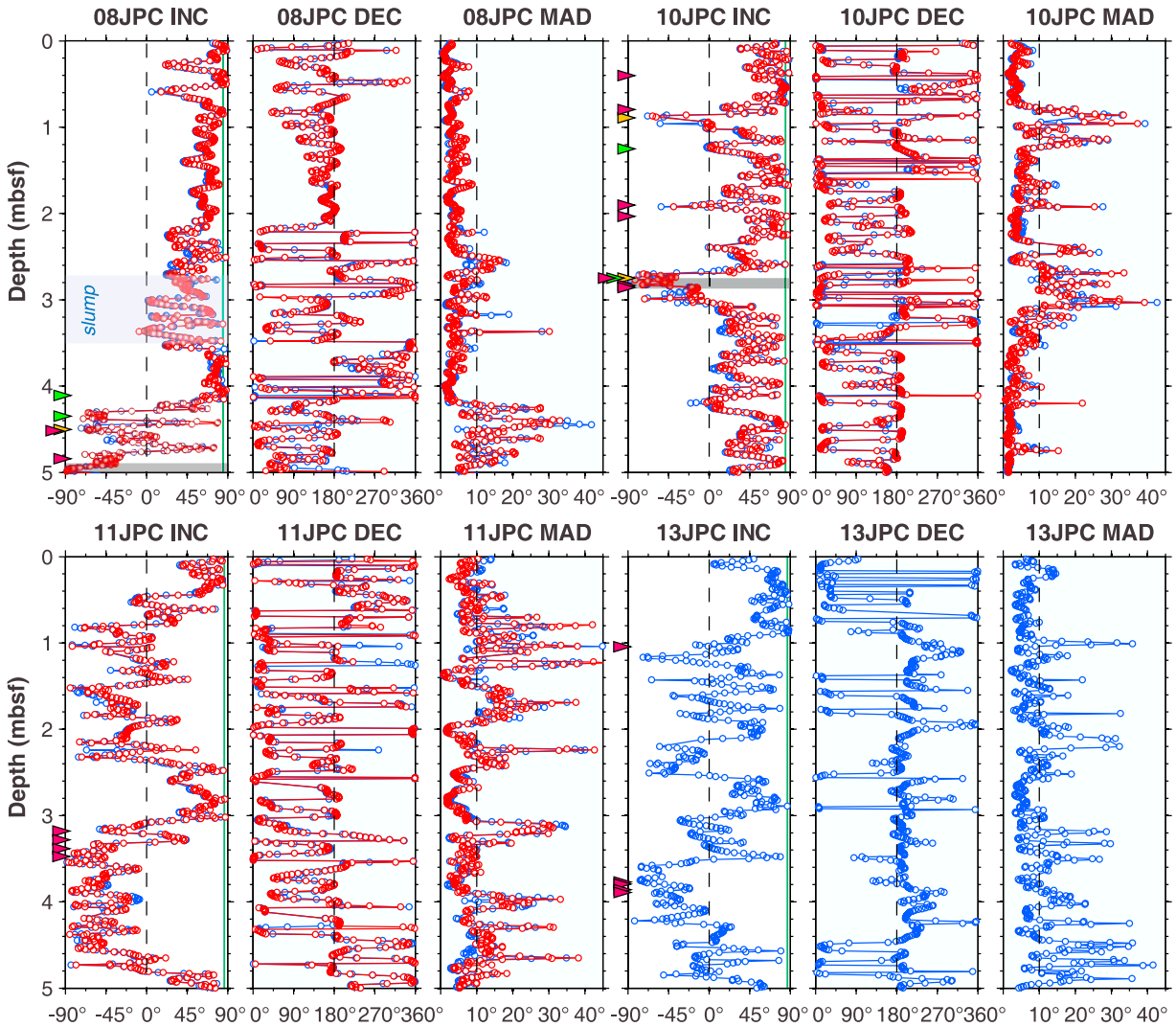

Figure 2. Component inclination and declination with maximum angular deviation (MAD) calculated for the 20–80 mT peak alternating field range for cores 08JPC, 10JPC, 11JPC, and 13JPC. Results calculated using data from XYZ and ZXY demagnetization sequences for the three sample axes are in blue and red, respectively. Note that core 13JPC samples were measured using only the XYZ demagnetization sequence. Declination values are arbitrary as cores were not oriented in azimuth. Dark gray shading indicates intervals from which magnetic extracts were taken. Red triangles represent depth levels where thermally demagnetized samples (Figure 3) were collected. Green (orange) triangles indicate depth levels where low- (high-) temperature data (Figures 5 and 6) were acquired. Vertical green lines are expected inclinations for a geocentric axial dipole field at the coring sites.

nence (ARM) acquisition during AF demagnetization. The first XYZ demagnetization sequence was followed by measurement, and then the ZXY demagnetization sequence was followed by repeat measurement at the same demagnetization step. As there was no discernable affect with differing order of demagnetization, only the XYZ demagnetization sequence was applied to samples from core 13JPC. Component magnetization directions for these cores were calculated from the 20–80 mT demagnetization peak field interval using the principle component analysis (PCA) method [*Kirschvink*, 1980]. For the uppermost 5 mbsf, component inclinations of these cores are characterized by several negative inclination intervals that reach thicknesses of several tens of centimeters (Figure 2). The maximum angular deviation (MAD) values associated with the PCA calculations are often lower than 10° (Figure 2), especially for cores 08JPC and 10JPC, indicating reasonably well defined component directions (Figure 3). However, component inclinations from these cores are generally tens of degrees lower than the expected inclinations for a geocentric axial dipole field at

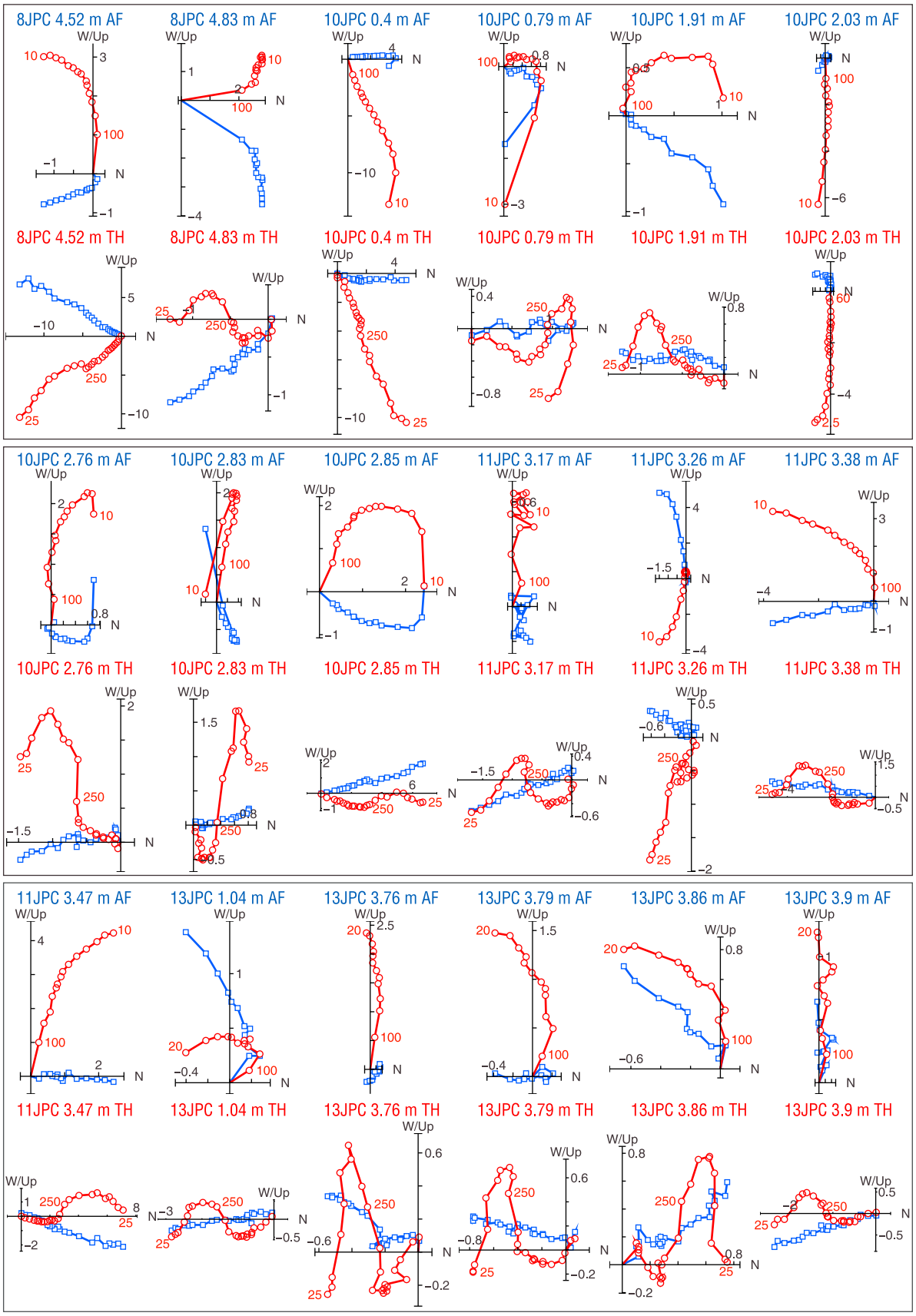
8JPC 4.52 m AF
8JPC 4.83 m AF
10JPC 0.4 m AF
10JPC 0.79 m AF
10JPC 1.91 m AF
10JPC 2.03 m AF
8JPC 4.52 m TH
8JPC 4.83 m TH
10JPC 0.4 m TH
10JPC 0.79 m TH
10JPC 1.91 m TH
10JPC 2.03 m TH
10JPC 2.76 m AF
10JPC 2.83 m AF
10JPC 2.85 m AF
11JPC 3.17 m AF
11JPC 3.26 m AF
11JPC 3.38 m AF
10JPC 2.76 m TH
10JPC 2.83 m TH
10JPC 2.85 m TH
11JPC 3.17 m TH
11JPC 3.26 m TH
11JPC 3.38 m TH
11JPC 3.47 m AF
13JPC 1.04 m AF
13JPC 3.76 m AF
13JPC 3.79 m AF
13JPC 3.86 m AF
13JPC 3.9 m AF
11JPC 3.47 m TH
13JPC 1.04 m TH
13JPC 3.76 m TH
13JPC 3.79 m TH
13JPC 3.86 m TH
13JPC 3.9 m TH
W/Up
N

Figure 3

the coring sites (vertical green lines in Figure 2). Although a slump or gravity flow deposit distorts the record at 2.7–3.5 mbsf in core 08JPC [*Adler et al.*, 2009], slumps have not otherwise been detected in these cores. No significant differences were observed between component directions calculated using data from the two separate demagnetization sequences (XYZ and ZXY, blue and red curves in Figure 2, respectively), precluding the possibility of negative inclinations being caused by spurious ARM acquisition during AF demagnetization.

[5] Age control for core 08JPC was obtained from radiocarbon dating (uppermost ~70 cm), amino acid racemization methods [*Kaufman et al.*, 2008], correlation with cores from the Lomonosov Ridge, and correlation of supposed glacial intervals with glaciations of the Eurasian Arctic margin [*Adler et al.*, 2009]. The uppermost 5 m of core 08JPC was estimated to span the last ~250 kyr. This and other sediment cores from the Mendeleev-Alpha Ridge have been correlated using paleomagnetic inclination patterns (of uncertain origin), detrital carbonate abundance, and the top of the predominantly brown sediment with an estimated age of ~500 kyr [*Polyak et al.*, 2009]. This marked color change was recovered at 8–10 mbsf in cores on the southern Mendeleev Ridge (e.g., core 08JPC), and at 4–6 mbsf in cores from the interior of the western Arctic Ocean (e.g., cores 10JPC, 11JPC, and 13JPC). The resulting sedimentation rate of ~1–2 cm/kyr is consistent with the cm/kyr scale sedimentation rate that has been suggested for this area [e.g., *Backman et al.*, 2004; *Spielhagen et al.*, 2004]. In summary, the top 5 m of the studied cores can be constrained to the Brunhes Chron, restricting the observed negative inclinations to diagenetic or sedimentological artifacts, or to magnetic excursions of Brunhes age. No correlation was found for intervals of negative NRM inclination with visual color, or with magnetic concentration parameters such as susceptibility, anhysteretic remanence (ARM) and isothermal remanence (IRM), or with magnetic grain size proxies.

[6] The NRMs of discrete ($2 \times 2 \times 2$ cm^3) samples collected in cubic plastic boxes alongside the u channel samples were measured during thermal demagnetization. The discrete samples were dried in a magnetically shielded space with flowing helium gas before being taken out from the plastic containers and wrapped in Al foil for thermal treatment. Magnetizations were monitored before and after the drying and wrapping, and no significant differences were found. Magnetizations of the discrete samples were then measured after thermal treatments in 25°C steps in the 50–600°C temperature range. For samples that show steep positive AF-derived inclinations from u channel data, e.g., sample "10JPC 2.03 m AF" (Figure 3), the thermally demagnetized sample from the same depth level (i.e., "10JPC 2.03 m TH") shows similar demagnetization behavior (Figure 3). Samples with steep positive AF-derived inclinations are rarely seen in these sediments (Figure 2). For samples with shallow positive AF-derived inclinations, e.g., sample "10JPC 0.4 m AF" (Figure 3), thermal demagnetization indicates a hint of overlapping components at ~300°C (see "10JPC 0.4 m TH" in Figure 3). For samples characterized by negative AF-derived inclinations, thermal demagnetization often reveals multiple NRM components with negative inclination components having unblocking temperatures largely below 350°C (e.g., sample "10JPC 2.83 m TH"), but occasionally reaching 500°C (e.g., sample "10JPC 1.91 m TH" in Figure 3). The negative inclination component is superimposed on a higher unblocking temperature (up to 600°C) component with positive inclination that may have a direction close to the direction of the geomagnetic field at time of sediment deposition. It appears that the negative inclination components, resolved by AF demagnetization (Figures 2 and 3), are carried by a magnetic mineral(s) that has unblocking temperatures largely below 350°C. A soft component with positive inclinations is also apparent in the 50–175°C demagnetization range. This low unblocking temperature component could be coring-derived and/or a viscous remanence (VRM). NRM intensity measured during thermal treatment for samples presented in Figure 3 show an inflexion at ~300°C (Figure 4), corresponding to the unblocking of a

Figure 3. Orthogonal projection of thermal demagnetization (red labels) for discrete cubic (~$2 \times 2 \times 2$ cm^3) samples from cores 08JPC, 10JPC, 11JPC, and 13JPC, compared to orthogonal projection of alternating field demagnetization (blue labels) for u channel intervals from the same depth level. Peak demagnetizing field ranges are 10–60 mT in 5 mT steps then 60–100 mT in 10 mT steps for cores 08JPC, 10JPC, and 11JPC. For core 13JPC, peak demagnetization fields are 20–60 mT in 5 mT steps then 60–100 mT in 10 mT steps. Temperature ranges are 25°C–600°C in 25°C steps for all samples. Circles (red) and squares (blue) denote projection on vertical and horizontal planes, respectively. Declination values are arbitrary as cores were not oriented in azimuth. Unit for intensity scale is mA/m. Meter levels correspond to meters below seafloor (mbsf) of each core as in Figure 2.

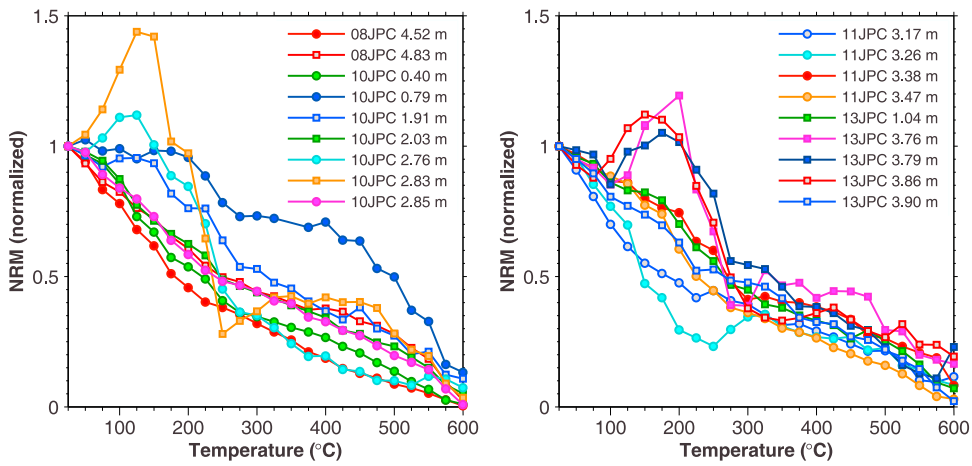

Figure 4. NRM intensity variation during thermal demagnetization for samples presented in Figure 3. NRM intensity data have been normalized by the NRM intensity value at room temperature (25°C) of each sample.

component observed in the orthogonal projections of Figure 3. The inflexion is more apparent in samples with negative AF-derived inclination (e.g., "10JPC 2.76 m," "10JPC 2.83 m"), and less apparent for samples with positive AF-derived inclination (i.e., "10JPC 0.4 m" and "10JPC 2.03 m").

3. Rock Magnetic Studies

[7] To identify the magnetic minerals in these sediments, rock magnetic experiments have been conducted at high (room temperature to 700°C) and low (20 K to room temperature) temperatures at the Institute for Rock Magnetism (IRM) at the University of Minnesota. Hysteresis loops were measured at 25°C temperature steps ranging from room temperature up to 700°C, in a helium atmosphere, on a vibrating sample magnetometer (VSM) for selected samples from cores 08JPC and 10JPC (see Figure 2). Samples were freeze dried, powdered, cemented, and stuck to a ceramic holder, prior to the VSM measurements. Saturation magnetization (Ms) derived from the hysteresis loops after slope correction, reveals abrupt drops below 300°C and below 600°C (Figure 5a), indicating two magnetic phases. The coercivity of remanence (Bcr) measured using backfield curves show a minimum at ~250°C, followed by a slight increase and a small peak at ~400°C (Figure 5b). For two samples from core 08JPC, magnetization was monitored at 1°C steps during cooling from 700°C to room temperature, in a 0.4 T field, after heating during hysteresis loop measurements. The magnetization acquired during cooling is about one order of magnitude higher than the magnetization prior to heating (Figure 5c). This dramatic increase of magnetization implies that a strongly magnetic phase has been produced during the heating. For selected freeze-dried bulk sediment samples (see Figure 2), room temperature saturation isothermal remanences (RT-SIRM), acquired in a 2.5 T field, were monitored using a Quantum Designs Magnetic Properties Measurement System (MPMS) on cooling to 20 K and subsequent warming to room temperature (Figure 6a). In addition, field cooled (FC) and zero-field cooled (ZFC) low-temperature SIRMs were measured on warming from 20 K to room temperature (Figure 6b). The FC remanences were measured after cooling in a 2.5 T field. For the ZFC remanences, samples were cooled in a zero field, and a 2.5 T field was applied at 20 K and then turned off prior to measurement on warming.

[8] The Ms against temperature (Ms(T)) data from cores 08JPC and 10JPC sediments (Figure 5a) are similar to those observed from sediments of core 06JPC [*Channell and Xuan*, 2009, Figure 5]. The abrupt drop of Ms just below 600°C indicates the presence of magnetite. This magnetite phase is probably a mixture of the original magnetite in the sediments and magnetite that has been produced during the heating. A much smaller contribution of magnetite to the IRM remanence [*Channell and Xuan*, 2009, Figure 4], and the huge increase of magnetization observed during the cooling (Figure 5c), as well as the suppressed Verwey transition in low-temperature data (Figure 6) suggest that the drop of Ms just below 600°C is mainly due to the magnetite produced during heating. Although titanomagnetite could exhibit the abrupt drop in Ms at ~300°C, the titanium content and grain size of titanomagnetite in the sediments would need to be very restricted to yield repeatable

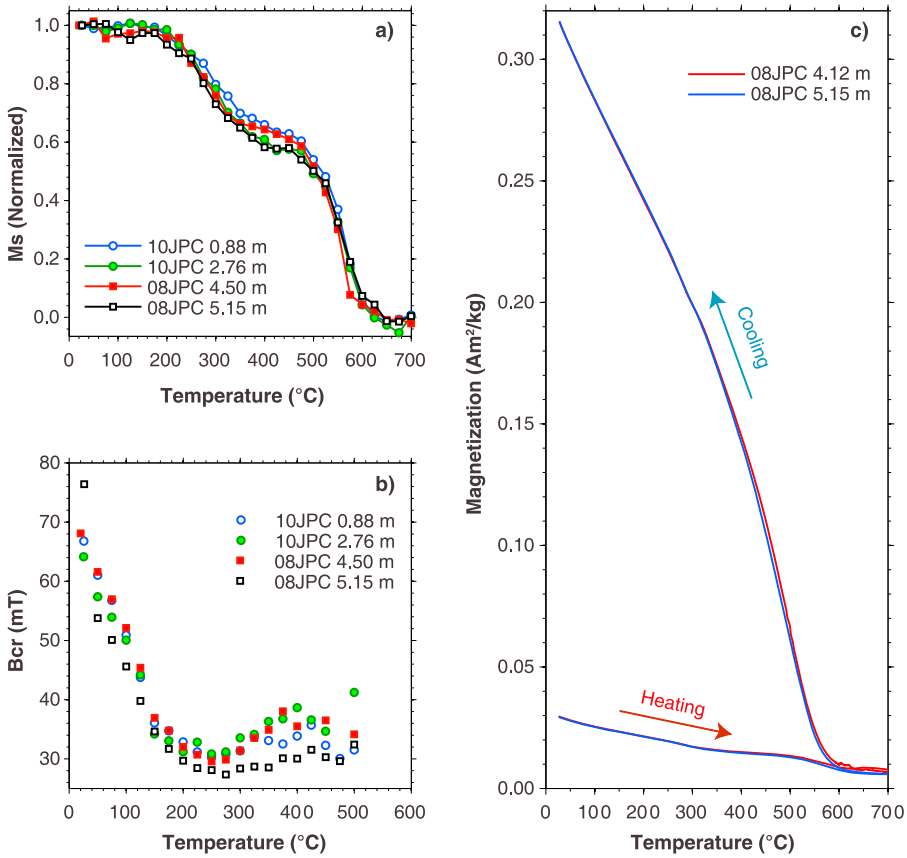

Figure 5. (a) Saturation magnetization (Ms) derived from hysteresis loops (saturation field of 0.4 T) measured at increasing temperatures (in 25°C steps in helium atmosphere) using a vibrating sample magnetometer (VSM). Values have been normalized to saturation magnetization at room temperature. (b) Coercivity of remanence (Bcr) measured using backfield curves (saturation field of 0.4 T) at increasing temperatures using VSM. (c) Magnetization in a 0.4 T applied field measured for two samples from core 08JPC during heating and cooling. Magnetizations during heating were derived from the hysteresis loops measured at 25°C–600°C in 25°C steps. Magnetizations during cooling were measured at each ~1°C step. Refer to Figure 2 for positions of samples in each core.

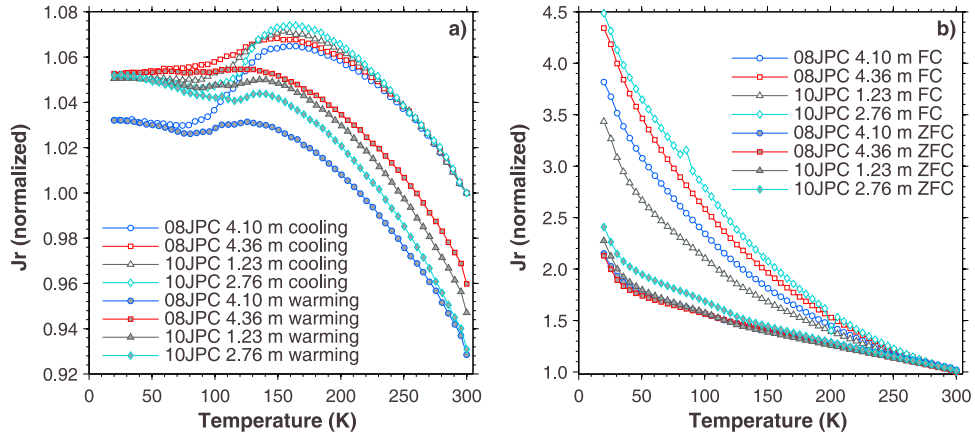

Figure 6. (a) Saturation isothermal remanent magnetization (SIRM), acquired in a 2.5 T field at room temperature, on cooling (open symbols) and warming (closed symbols), measured using a Quantum Designs Magnetic Properties Measurement System (MPMS). Measurements have been normalized to the room temperature magnetization of the samples on cooling. (b) Field (2.5 T) cooled (FC, open symbols) and zero field cooled (ZFC, closed symbols) low-temperature SIRM measured on warming. Measurements have been normalized to the field cooled magnetization of the samples at room temperature.

drops in Ms in the same temperature interval (i.e., ~300°C) for different samples. Titanomagnetite in deep-sea sediments usually has a range of titanium content and grain size leading to a range of unblocking temperatures. We therefore interpret the abrupt drop of Ms at ~300°C to the inversion of titanomaghemite. Titanomaghemite is metastable when heated above 250–300°C, and, when heated up to 600°C, the inversion product typically leads to increased Ms due to intergrowths of various minerals including magnetite and ilmenite [*Readman and O'Reilly*, 1972; *O'Reilly*, 1983; *Özdemir*, 1987; *Dunlop and Özdemir*, 1997; *Krása and Matzka*, 2007], explaining the observations in Figure 5c. The fact that the abrupt increase of magnetization during cooling occurs in a temperature interval (~400–580°C) lower than the temperature associated with the magnetization decrease on heating (~500–600°C) is consistent with the two stage inversion observed in synthetic titanomaghemite samples during heating and cooling [*Özdemir*, 1987]. The minimum in Bcr at ~250°C probably indicates the start of the titanomaghemite inversion (Figure 5b). The changes of Bcr during ~250–500°C may represent a blend between the generation of the new magnetic phase and the "unblocking" of preexisting magnetic grains. Partial oxidation of magnetite is known to smear the Verwey transition in magnetite from an abrupt drop at ~120 K to a wider temperature range [e.g., *Özdemir et al.*, 1993], consistent with our observation in the Arctic sediments (Figure 6). The humped cooling and warming curves of RT-SIRM between room temperature and the Verwey transition (Figure 6a) are believed to be diagnostic of partially oxidized magnetite grains characterized by maghemitized rims [*Özdemir and Dunlop*, 2010]. Titanomaghemite in the Arctic sediments might be produced through seafloor temperature diagenetic oxidation of titanomagnetite. The low sediment accumulation rate (cm/kyr scale) and low concentration of labile organic matter appear to provide the conditions for diagenetic oxidation.

[9] To further understand the magnetic mineralogy of the sediments, magnetic extracts were made from cores 08JPC and 10JPC using sediments from intervals characterized by negative AF-derived NRM inclinations (see Figure 2). The extracts were made by dispersing ~2 × 2 × 10 cm^3 sediment (~45 g) taken from the u channel samples in a sodium metaphosphate solution of 4 wt.%, and using an automated extraction system to separate magnetic particles. The extraction system is equipped with a peristaltic pump so that the sediment slurry can repeatedly flow next to a glass tube filled with strong rare earth magnets. The acquired extracts were then intermittently washed into a glass container using distilled water until no further extraction was achieved. A string of rare earth magnets in a glass test tube was then used to refine the extract. Extracts were again washed using distilled water, then methanol, and dried for isothermal remanence magnetization (IRM) acquisition measurements.

[10] IRM acquisition by the magnetic extracts was measured at one hundred equidistant field steps on a logarithmic scale ranging from ~7 mT to 1 T, using an alternating gradient magnetometer (AGM) at the University of Florida. Decomposition of the gradient of IRM acquisition curves provides a nondestructive tool for discriminating magnetic phases in natural samples [e.g., *Kruiver et al.*, 2001; *Heslop et al.*, 2002]. The method relies on the assumption that the IRM gradient can be approximated by addition of log Gaussian functions that represent individual coercivity components [*Robertson and France*, 1994] although this may not always be the case [see *Egli*, 2003]. IRM acquisition data of the magnetic extracts were analyzed following the method of *Heslop et al.* [2002]. Gradients of IRM acquisition data plotted on a log scale show apparent asymmetry in shape, indicative of multiple coercivity components (Figure 7). Satisfactory fits were achieved by modeling the gradient of the IRM acquisition data using two magnetic coercivity components (Figure 7), although grain interactions could also be responsible for this asymmetry [*Heslop et al.*, 2004]. Data from magnetic extract of core 10JPC sediments yields two components with mean coercivity of 55.6 mT and 106.6 mT, comparable to 55.5 mT and 101.5 mT obtained from core 08JPC magnetic extracts.

[11] The low- and high-coercivity components are consistent with the presence of (titano)magnetite and titanomaghemite, respectively. Theoretical modeling has shown that grain size thresholds for superparamagnetic to single domain (SD), SD to pseudo–single domain (PSD), and PSD to multidomain (MD) behaviors increase with increasing magnetite-maghemite oxidation state [*Moskowitz*, 1980]. Consequently, grains with certain size may change their domain state from MD to PSD or SD during the oxidation, thereby increasing their coercivities. Elevated coercivity has been observed for synthetic SD titanomagnetite grains with increasing oxidation parameter (z) up to ~0.5 [*Özdemir and*

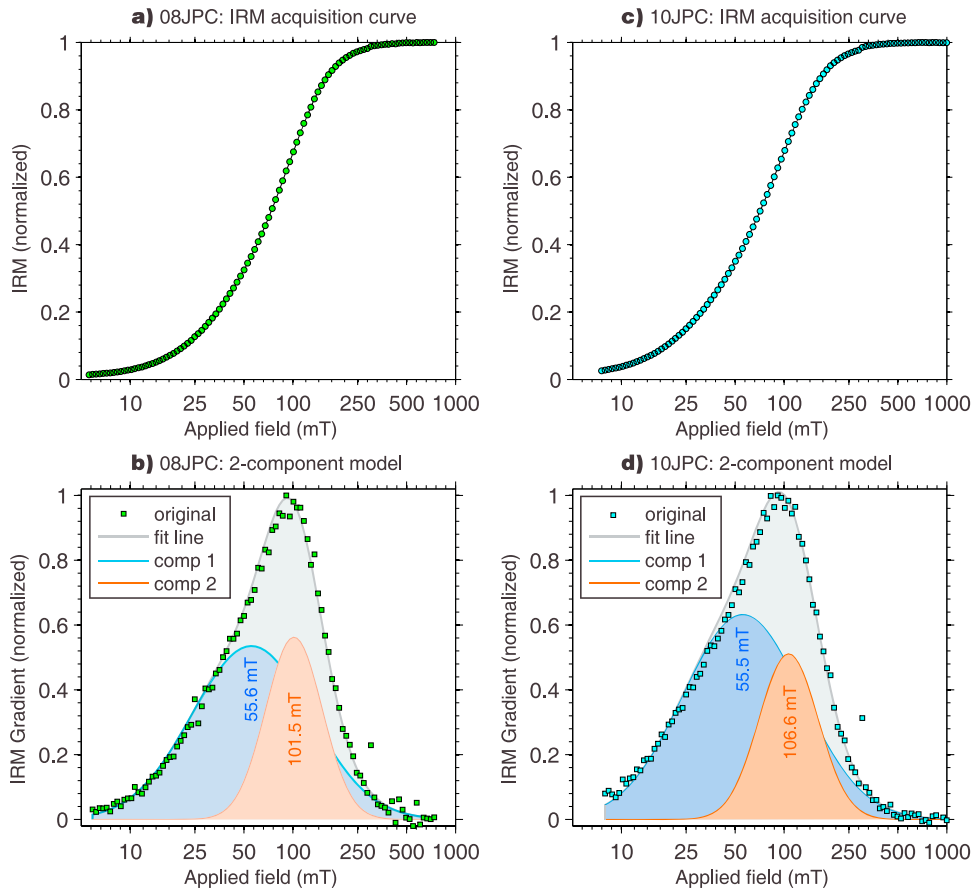

Figure 7. IRM acquisition curves for magnetic extracts from (a) core 08JPC and (c) core 10JPC, measured using an alternating gradient magnetometer (AGM), and two-component modeling of the IRM gradient data for magnetic extracts from (b) 08JPC and (d) 10JPC using the method of *Heslop et al.* [2002].

O'Reilly, 1982]. Further oxidation seems to cause a decrease of coercivity for the synthetic samples. In nature, coercivity of titanomaghemites is higher than that of unoxidized titanomagnetites for high z values [*Dunlop and Özdemir*, 1997]. Increases in coercivity observed in hysteresis loops [e.g., *Marshall and Cox*, 1972; *Beske-Diehl and Soroka*, 1984] or in median destructive field (MDF) from AF demagnetization [e.g., *Ryall et al.*, 1977; *Petersen and Vali*, 1987] are generally seen for natural titanomaghemite in ocean basalts with increasing oxidation sate. It is also likely that the oxidation of titanomagnetite to titanomaghemite preferentially occurs in finer grains that generally have larger surface area to volume ratio, leaving the larger grains less altered. Therefore, the titanomaghemite component may tend to have smaller grain size and hence higher coercivity than the titanomagnetite component. Additionally, partial oxidation that only affects the surfaces of the titanomagnetite particles could cause oxidation gradients and create stress that can substantially increase particle coercivity.

4. SEM and XRD Analyses

[12] Magnetic extracts spread on a carbon tape were examined under a Zeiss EVO scanning electron microscopy (SEM) equipped with Genesis X-ray energy dispersive spectroscopy (EDS) at the University of Florida. Elemental maps were collected on micron-sized grain clusters for up to 20 h using the EDS. The results show a number of grains that are rich in O, Ti, and Fe, consistent with the presence of (titano)magnetite and/or titanomaghemite. Calculation using the total image spectra acquired during the mapping yields mean composition parameters with x values of 0.35 and 0.45 for magnetic extracts from cores 08JPC and 10JPC, respectively. The Ti concentration apparently varies widely from one grain to another (Figure 8),

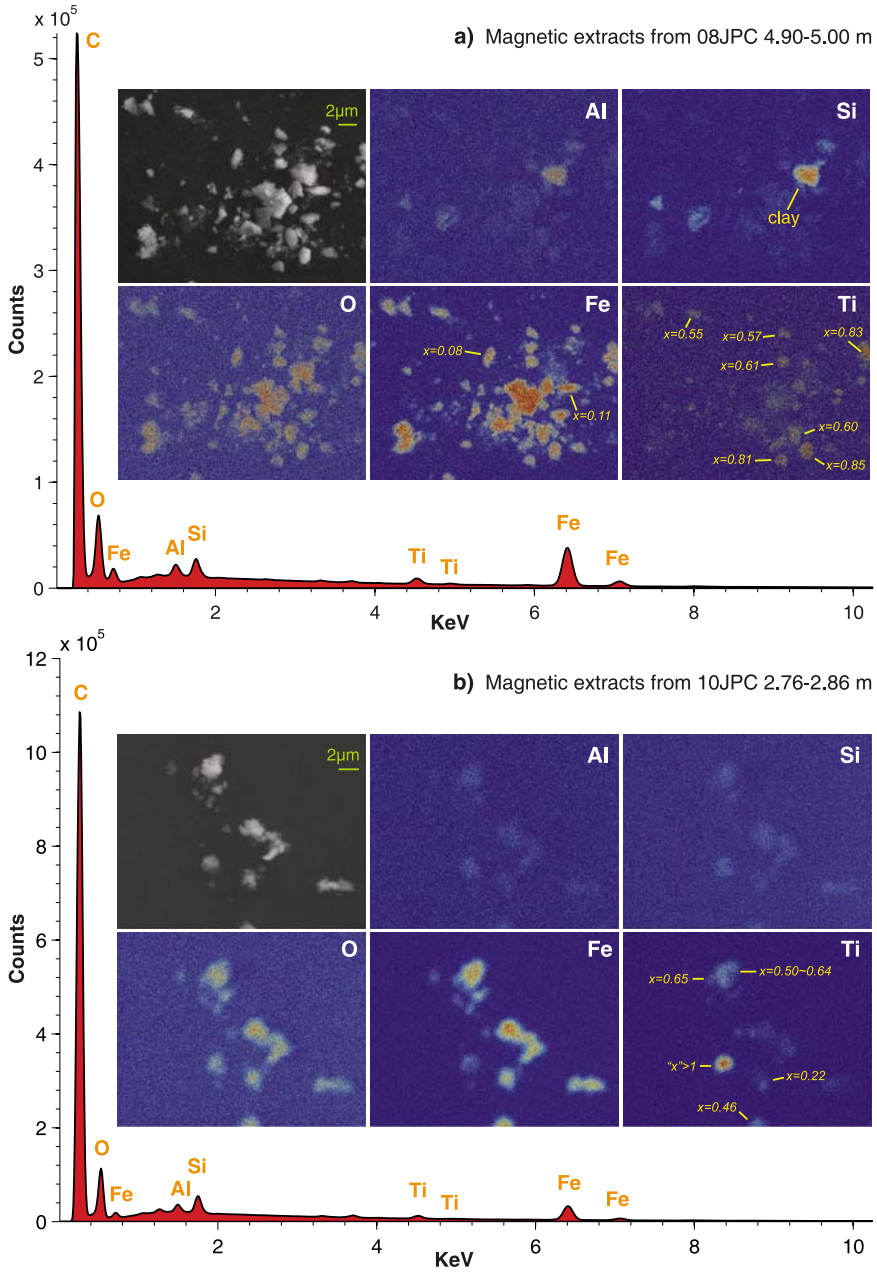

Figure 8. Scanning electron microscopy (SEM) and X-ray energy dispersive spectroscopy (EDS) analyses for micron-sized grains of magnetic extracts from cores (a) 08JPC and (b) 10JPC sediments. The image comprises (titano)magnetite and/or titanomaghemite grains with various Ti contents with x values up to 0.85 and clay minerals. The total image spectrum acquired during the mapping is also displayed, where the carbon peak is attributed to the carbon tape background.

with calculated Ti composition (x) ranging from 0.08 to 0.85 (Figure 8). The huge C peak is due to the carbon tape, and the Si, Al, and O rich grains can be attributed to quartz and clay minerals that were not completely removed during the extraction. The collected X-ray spectrum and the elemental map for magnetic extracts from core 08JPC are similar to those of core 10JPC, implying similar magnetic mineralogy for sediments in these cores.

[13] X-ray diffraction (XRD) analyses were performed on freeze-dried bulk sediment powders and on the magnetic extracts using a Rigaku Ultima IV X-ray diffractometer at the University of Florida. Magnetic extracts were placed on a zero background sample holder, and the "focusing beam" option was used for all measurements. High-resolution diffraction patterns were collected in the 10–90° 2θ range for the bulk sediment powders, and in

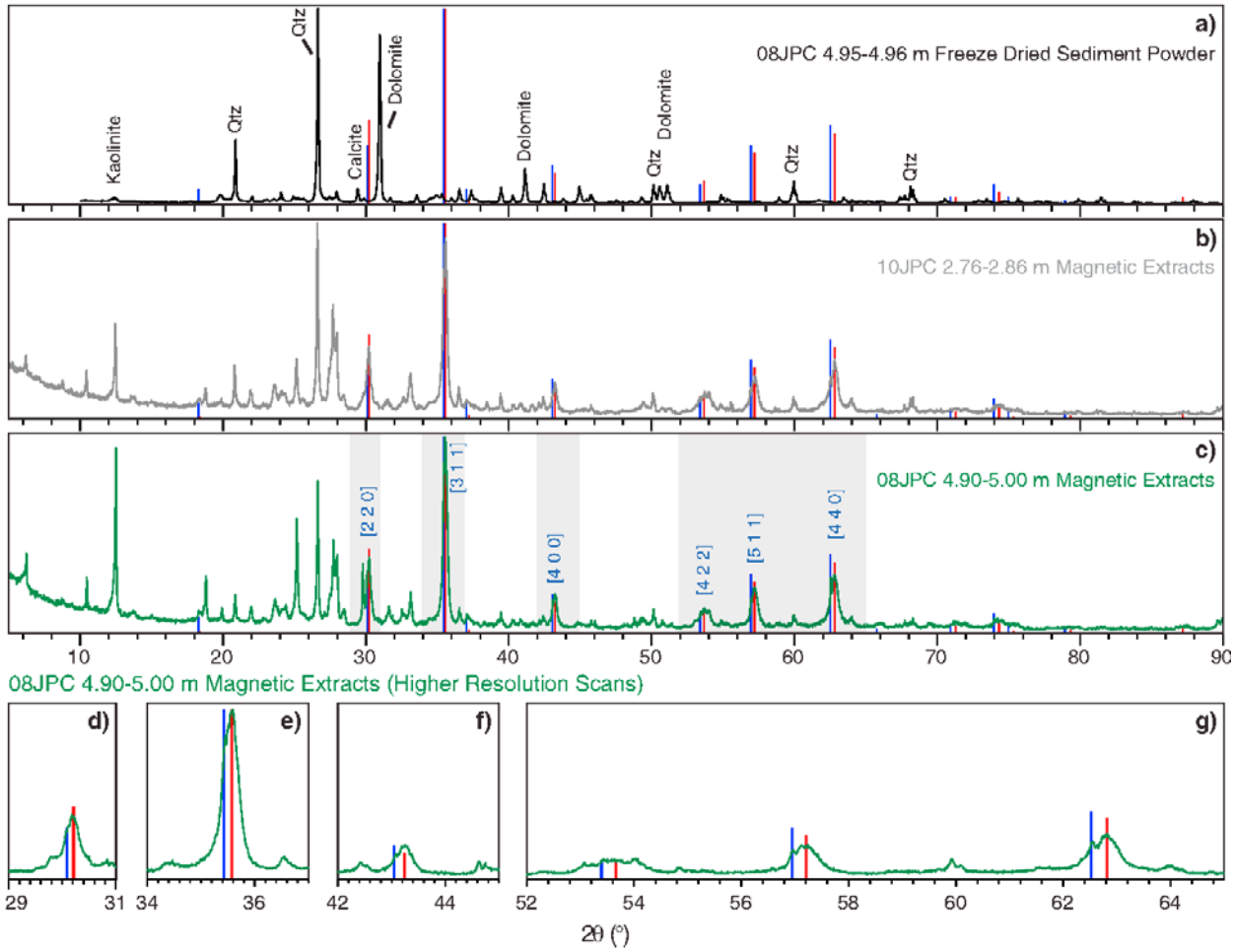

Figure 9. X-ray diffraction (XRD) results for (a) freeze-dried bulk sediment powders from core 08JPC (black) and magnetic extracts from cores (b) 10JPC (gray) and (c) 08JPC (green), with (d–g) higher-resolution scans around the major peaks associated with titanomaghemite and (titano)magnetite. The 2θ positions and magnitudes of XRD peaks for synthetic magnetite and titanomaghemite standards are indicated by vertical blue and red lines, respectively. QTz denotes quartz.

the 5–90° 2θ range for magnetic extracts, using a 0.02° step size and a 10 s count time for each step. The results for bulk sediments were dominated by quartz and dolomite peaks (Figure 9a). Detrital carbonate is common in these sediments and dolomite-rich layers are a lithostratigraphic feature of sediments across the western Arctic Ocean [e.g., *Polyak et al.*, 2009]. Magnetic phases in the bulk sediments are not detectable from the XRD data due to their low concentrations. The two magnetic extract samples show very similar diffraction patterns. The major peaks are consistent with a synthetic magnetite standard, and the titanomaghemite standard reported from pillow basalts of

Table 2. The 2θ Values and Estimated Lattice Parameters for (Titano)magnetite and Titanomaghemite Derived by Modeling of the Six High-Resolution X-Ray Diffraction Peaks in Figures 9d–9g

		Diffraction Plane						
Components	Parameters[a]	[2 2 0]	[3 1 1]	[4 0 0]	[4 2 2]	[5 1 1]	[4 4 0]	Mean
(Titano)magnetite	2θ (deg)	30.0595	35.4414	43.0767	53.4418	56.9510	62.5559	
	L.P. (Å)	8.4015	8.3933	8.3926	8.3924	8.3948	8.3926	8.3945
Titanomaghemite	2θ (deg)	30.1830	35.5376	43.2078	53.7190	57.1725	62.7973	
	L.P. (Å)	8.3679	8.3713	8.3683	8.3523	8.3650	8.3636	8.3647

[a] L.P., lattice parameters.

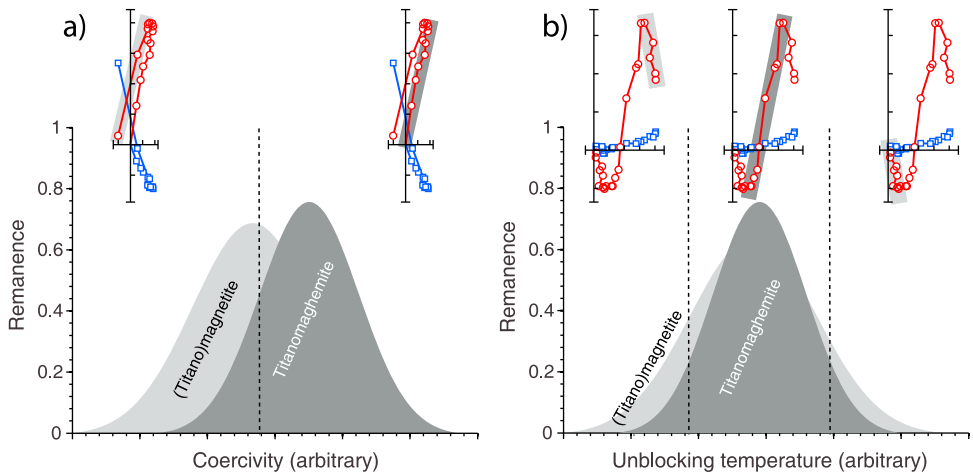

Figure 10. Conceptual models for (a) the coercivity spectra and (b) the unblocking temperature spectra that can explain typical demagnetization behavior exhibited in Figure 3, using orthogonal projections for sample "10JPC 2.83 m." In this model, the (titano)magnetite carries a primary magnetization (DRM), and the titanomaghemite carries a partially self-reversed CRM.

mid-Atlantic Ocean [*Xu et al.*, 1997]. Two closely overlapping yet distinct peaks that correspond to magnetite (blue lines in Figure 8) and titanomaghemite (red lines in Figure 8) can be recognized for all dominant diffraction planes (Figures 9b and 9c). Diffraction patterns of magnetic extracts also show peaks corresponding to quartz and clay minerals such as kaolinite, consistent with EDS observations. Higher-resolution diffraction patterns were collected for magnetic extracts within four 2θ intervals (i.e., 29–31°, 34–37°, 42–44.5°, 52–65°) that cover the dominant peaks of magnetite and titanomaghemite associated with the [2 2 0], [3 1 1], [4 0 0], [4 2 2], [5 1 1], and [4 4 0] diffraction planes. A 0.01° step size and a 20 s count time were used for the analyses. It is clear that the observed peaks on these diffraction planes comprise two distinct peaks that fit (titano)magnetite and titanomaghemite (Figures 9d–9g). Calculated lattice parameters (Table 2) using the higher-resolution XRD data give an average value of 8.3945 Å for the (titano)magnetite component and 8.3647 Å for the titanomaghemite component. The lattice parameters for the titanomaghemite component are sufficiently low that the oxidation states (z) must be >0.9 for a wide range of Ti contents or x values [see *Readman and O'Reilly*, 1972; *Nishitani and Kono*, 1983].

5. Discussion

[14] Thermal demagnetization of the NRM implies that negative inclination components resolved by AF demagnetization are carried by a magnetic phase that has unblocking temperatures largely below 350°C. Rock magnetic studies, SEM and EDS observations, and XRD analyses, on sediments and magnetic extracts, reveals the presence of titanomaghemite and (titano)magnetite in these Arctic sediments, consistent with the results from core 06JPC [*Channell and Xuan*, 2009]. The negative NRM inclination component is apparently carried by the titanomaghemite that has slightly higher coercivity (AF demagnetization) than (titano)magnetite, and "unblocking" temperatures (thermal demagnetization) largely below 350°C due to inversion upon heating. Typical AF and thermal demagnetization behavior observed in Figure 3 (e.g., that of sample 10JPC 2.83 m) can be explained using a conceptual model in which coercivity and unblocking temperature spectra for the titanomaghemite and (titano)magnetite components are represented as being distributed as Gaussian functions (Figure 10). Note that the low-coercivity and the low unblocking temperature part on the spectra may be susceptible to VRM. Titanomaghemite is known to have a propensity for acquisition of VRM [e.g., *Özdemir and Banerjee*, 1981], and Arctic sediments have been noted for their ability to acquire VRM that often resists moderate peak AF fields, up to >20 mT [e.g., *Løvlie et al.*, 1986; *Witte and Kent*, 1988]. The low-coercivity (generally <20 mT) and low unblocking temperature (<175°C) component with positive inclinations (Figure 3) may be drilling related and/or a VRM, or possibly a detrital remanent magnetization (DRM) carried by original (titano)magnetite with larger grain sizes (lower coercivities), or a mixture of remanence types.

[15] The excessive thickness (up to >40 cm) of negative inclination (AF-derived) intervals in the studied cores and the lack of a comparable patterns from core to core (Figure 2) means that the observed negative inclinations cannot be satisfactorily ascribed to geomagnetic excursions. The negative inclination component carried by titanomaghemite could originate as a self-reversed CRM formed during the low-temperature oxidation of the original detrital (titano)magnetite grains to titanomaghemite [*Channell and Xuan*, 2009]. The possibility of self-reversed CRM in titanomaghemite has been discussed since 1950s. It was suggested [*Verhoogen*, 1956, 1962; *O'Reilly and Banerjee*, 1966] that self-reversal can be accomplished by ionic reordering of the two sublattices in titanomagnetite during oxidation. Prior to oxidation, the B (octahedral) sublattice in titanomagnetite has a higher spontaneous magnetization than the A (tetrahedral) sublattice. During the oxidation, cation vacancies only form in B sublattice, and the inverse magnetization of the A sublattice could eventually become the stronger, causing the self-reversal. Partial and complete self-reversals have been reported in oceanic basalts [*Doubrovine and Tarduno*, 2004, 2006a], carried by titanomaghemite with N-type thermomagnetic properties, and were attributed to CRM acquired during the oxidation of titanomagnetite by ionic reordering. Theoretical models of the maghemitization process [*O'Reilly and Banerjee*, 1966] and studies on compositions of titanomaghemite with/without self-reversal observations [*Doubrovine and Tarduno*, 2005, 2006a, 2006b] suggest that a limited range of high oxidation states ($z \geq 0.9$) and relatively high Ti contents ($x \geq 0.6$) are required to produce natural self-reversed components. High temperatures were thought to be required to achieve such high oxidation state [e.g., *O'Reilly and Banerjee*, 1966]; however, high temperatures may destroy the stability of the cation-deficient structure of titanomaghemite. Iron removal appears to be capable of producing the required oxidation states at seafloor temperatures, while maintaining the stability of the cation-deficient titanomaghemite lattice structure [e.g., *Doubrovine and Tarduno*, 2006a]. Self-reversal has also been reported in continental basalts containing oxidized titanomaghemite [*Krása et al.*, 2005]. In this case, reproduction of the self-reversals in laboratory thermoremanence leads the authors to preclude any long-term process such as ionic reordering as the responsible mechanism. The authors explained the observed self-reversals by magnetic coupling between the two magnetic phases with different unblocking temperatures (i.e., titanomagnetite and oxidized titanomaghemite), in a close side-by-side assemblage. Such a mechanism often requires specific geometry and magnetic properties of the associated magnetic phases, and the self-reversed component is carried by the magnetically softer titanomagnetite that has lower Curie temperatures [see *Krása et al.*, 2005], inconsistent with the observations in the Arctic sediments studied here.

[16] Although relatively low mean Ti contents with estimated mean x values of 0.35 and 0.45 were obtained from the EDS analyses, the existence of a population of Ti-rich iron oxide grains, presumably titanomaghemite, with elevated x values up to 0.85 is also apparent (Figure 8). Lattice parameters of the titanomaghemite in these Arctic sediments, estimated from XRD data (Figure 9 and Table 2), indicate high oxidation state ($z > 0.9$). These observations appear to favor the explanation that the self-reversed component is a titanomaghemite CRM produced by alteration of thermal remanent magnetization (TRM) carried by the original (titano)magnetite that contributed to the original DRM of the sediments. Statistically, the grains that carry the self-reversed CRM would alter (distort) the original DRM to a degree that depends on the abundance of affected grains, causing the observed negative inclination intervals and the generally shallow inclinations. Stratigraphic correlations of the negative inclination intervals among different cores from the Arctic Ocean [e.g., *Spielhagen et al.*, 2004; *Backman et al.*, 2004; *Kaufman et al.*, 2008; *Adler et al.*, 2009; *Polyak et al.*, 2009] indicate a primary lithological control on the degree of alteration, and hence on the position of zones of negative inclination.

6. Conclusions

[17] Several lines of evidence lead to the recognition of titanomaghemite and (titano)magnetite in these Arctic sediments. (1) Ms(T) curves show an abrupt drop below 300°C and 600°C. (2) There is a dramatic increase of magnetization during cooling of samples heated to 700°C. (3) There is a manifestation of a suppressed and thermally dispersed Verwey transition in low-temperature measurements including room temperature SIRM on cooling to 20 K and subsequent warming to room temperature and FC/ZFC curves measured on warming from 20 K to room temperature. (4) Decomposition of the gradient of IRM acquisition curves measured from magnetic extract samples is consistent with the presence of titanomaghemite and (titano)magnetite

that have slightly different coercivities. (5) Elemental maps collected using SEM and EDS on micron-sized grains of magnetic extracts confirm the existence of titanomaghemite/(titano)magnetite with various Ti contents. (6) High-resolution X-ray diffraction patterns of the magnetic extracts fit well with titanomaghemite and magnetite standards.

[18] Thermal demagnetization of NRM indicates that negative inclination components in these Arctic sediments are carried by titanomaghemite that has ''unblocking'' temperatures largely below 350°C due to inversion. SEM and EDS observation of high Ti content titanomaghemite/(titano)magnetite grains with estimated x values of up to 0.85, and high oxidation state with $z > 0.9$ estimated using lattice parameters calculated from the XRD data, provide the conditions for a certain proportion of titanomaghemite grains in the Arctic sediments to undergo self-reversal by ionic reordering. Although the possibility of unusual behavior of the paleomagnetic field in the Arctic area cannot be completely discarded, negative inclination intervals and shallow inclinations in these Arctic cores are most likely due to modifications of the original DRM by a self-reversed CRM carried by titanomaghemite formed during diagenesis from primary titanomagnetite grains.

Acknowledgments

[19] The Institute for Rock Magnetism (IRM) at the University of Minnesota provided Chuang Xuan a visiting fellowship for the high- and low-temperature rock magnetic work and assisted with data acquisition. We thank Leonid Polyak for facilitating the u channel and discrete sample collections at the Ohio State University. Ann Heatherington assisted with SEM and EDS analyses. Kainian Huang helped with the NRM thermal demagnetization experiments. This research was supported by the U.S. National Science Foundation through award ARC-0806309.

References

Adler, R., L. Polyak, J. D. Ortiz, D. S. Kaufman, J. E. T. Channell, C. Xuan, A. G. Grottoli, E. Sellen, and K. A. Crawford (2009), Sediment record from the western Arctic Ocean with an improved Late Quaternary age resolution: HOTRAX core HLY0503-8JPC, Mendeleev Ridge, *Global Planet. Change*, *68*, 18–29, doi:10.1016/j.gloplacha.2009.03.026.

Backman, J., M. Jakobsson, R. Løvlie, L. Polyak, and L. A. Febo (2004), Is the central Arctic Ocean a sediment starved basin?, *Quat. Sci. Rev.*, *23*, 1435–1454, doi:10.1016/j.quascirev.2003.12.005.

Backman, J., et al. (2008), Age model and core-seismic integration for the Cenozoic Arctic Coring Expedition sediments from the Lomonosov Ridge, *Paleoceanography*, *23*, PA1S03, doi:10.1029/2007PA001476.

Beske-Diehl, S. J., and W. L. Soroka (1984), Magnetic properties of variably oxidized pillow basalt, *Geophys. Res. Lett.*, *11*, 217–220, doi:10.1029/GL011i003p00217.

Bleil, U. (1987), Quaternary high latitude magnetostratigraphy, *Polar Res.*, *5*, 325–327, doi:10.1111/j.1751-8369.1987.tb00566.x.

Channell, J. E. T., and C. Xuan (2009), Self-reversal and apparent magnetic excursions in Arctic sediments, *Earth Planet. Sci. Lett.*, *284*, 124–131, doi:10.1016/j.epsl.2009.04.020.

Clark, D. L., R. R. Whitman, K. A. Morgan, and S. D. Mackay (1980), Stratigraphy and glacial-marine sediments of the basin, central Arctic Ocean, *Spec. Pap. Geol. Soc. Am.*, *181*, 1–57.

Clark, D. L., J.-S. Vincent, G. A. Jones, and W. A. Morris (1984), Correlation of marine and continental glacial and interglacial events, Arctic Ocean and Banks Island, *Nature*, *311*, 147–149, doi:10.1038/311147a0.

Darby, D. A., J. F. Bischof, and G. A. Jones (1997), Radiocarbon dating of depositional regimes in the western Arctic Ocean, *Deep Sea Res., Part II*, *44*, 1745–1757, doi:10.1016/S0967-0645(97)00039-8.

Doubrovine, P. V., and J. A. Tarduno (2004), Self-reversed magnetization carried by titanomaghemite in oceanic basalts, *Earth Planet. Sci. Lett.*, *222*, 959–969, doi:10.1016/j.epsl.2004.04.009.

Doubrovine, P. V., and J. A. Tarduno (2005), On the compositional field of self-reversing titanomaghemite: Constraints from Deep Sea Drilling Project Site 307, *J. Geophys. Res.*, *110*, B11104, doi:10.1029/2005JB003865.

Doubrovine, P. V., and J. A. Tarduno (2006a), Alteration and self-reversal in oceanic basalts, *J. Geophys. Res.*, *111*, B12S30, doi:10.1029/2006JB004468.

Doubrovine, P. V., and J. A. Tarduno (2006b), N-type magnetism at cryogenic temperatures in oceanic basalt, *Phys. Earth Planet. Inter.*, *157*, 46–54, doi:10.1016/j.pepi.2006.03.002.

Dunlop, D. J., and O. Özdemir (1997), *Rock Magnetism: Fundamentals and Frontiers*, 573 pp., Cambridge Univ. Press, New York.

Egli, R. (2003), Analysis of the field dependence of remanent magnetization curves, *J. Geophys. Res.*, *108*(B2), 2081, doi:10.1029/2002JB002023.

Gubbins, D. (1999), The distinction between geomagnetic excursions and reversals, *Geophys. J. Int.*, *137*, F1–F3, doi:10.1046/j.1365-246x.1999.00810.x.

Herman, Y. (1974), Arctic Ocean sediments, microfauna, and the climatic record in late Cenozoic time, in *Marine Geology and Oceanography of the Arctic Seas*, edited by Y. Herman, pp. 283–348, Springer, Berlin.

Heslop, D., M. J. Dekkers, P. P. Kruiver, and I. H. M. van Oorschot (2002), Analysis of isothermal remanent magnetization acquisition curves using the expectation-maximization algorithm, *Geophys. J. Int.*, *148*, 58–64, doi:10.1046/j.0956-540x.2001.01558.x.

Heslop, D., G. McIntosh, and M. Dekkers (2004), Using time and temperature dependant Preisach models to investigate the limitations of modelling isothermal remanent magnetisation curves with cumulative log Gaussian functions, *Geophys. J. Int.*, *157*, 55–63, doi:10.1111/j.1365-246X.2004.02155.x.

Hunkins, K., A. W. H. Bé, N. D. Opdyke, and G. Mathieu (1971), The Late Cenozoic history of the Arctic Ocean, in *The Late Cenozoic Glacial Ages*, edited by K. K. Turekian, pp. 215–237, Yale Univ. Press, New Haven, Conn.

Jakobsson, M., R. Løvlie, H. Al-Hanbali, E. Arnold, J. Backman, and M. Mörth (2000), Manganese and color cycles in Arctic Ocean sediments constrain Pleistocene chronology, *Geology*,

28, 23–26, doi:10.1130/0091-7613(2000)28<23:MACCIA>2.0.CO;2.

Jakobsson, M., J. Backman, A. Murray, and R. Løvlie (2003), Optically Stimulated Luminescence dating supports central Arctic Ocean cm-scale sedimentation rates, *Geochem. Geophys. Geosyst.*, *4*(2), 1016, doi:10.1029/2002GC000423.

Jakobsson, M., R. Macnab, M. Mayer, R. Anderson, M. Edwards, J. Hatzky, H.-W. Schenke, and P. Johnson (2008), An improved bathymetric portrayal of the Arctic Ocean: Implications for ocean modeling and geological, geophysical and oceanographic analyses, *Geophys. Res. Lett.*, *35*, L07602, doi:10.1029/2008GL033520.

Kaufman, D. S., L. Polyak, R. Adler, J. E. T. Channell, and C. Xuan (2008), Dating late Quaternary planktonic foraminifer *Neogloboquadrina pachyderma* from the Arctic Ocean by using amino acid racemization, *Paleoceanography*, *23*, PA3224, doi:10.1029/2008PA001618.

Kirschvink, J. L. (1980), The least squares lines and plane analysis of paleomagnetic data, *Geophys. J. R. Astron. Soc.*, *62*, 699–718.

Krása, D., and J. Matzka (2007), Inversion of titanomaghemite in oceanic basalt during heating, *Phys. Earth Planet. Inter.*, *160*, 169–179, doi:10.1016/j.pepi.2006.11.004.

Krása, D., V. P. Shcherbakov, T. Kunzmann, and N. Petersen (2005), Self-reversal of remanent magnetization in basalts due to partially oxidized titanomagnetites, *Geophys. J. Int.*, *162*, 115–136, doi:10.1111/j.1365-246X.2005.02656.x.

Kruiver, P. P., M. J. Dekkers, and D. Heslop (2001), Quantification of magnetic coercivity components by the analysis of acquisition curves of isothermal remanent magnetisation, *Earth Planet. Sci. Lett.*, *189*, 269–276, doi:10.1016/S0012-821X(01)00367-3.

Laj, C., and J. E. T. Channell (2007), Geomagnetic excursions, in *Treatise on Geophysics*, vol. 5, edited by G. Schubert, pp. 373–416, Elsevier, Amsterdam.

Løvlie, R., B. Markussen, H. P. Sejrup, and J. Thiede (1986), Magnetostratigraphy in three Arctic Ocean sediment cores; arguments for magnetic excursions within oxygen isotope stage 2–3, *Phys. Earth Planet. Inter.*, *43*, 173–184, doi:10.1016/0031-9201(86)90084-1.

Marshall, M., and A. Cox (1972), Magnetic changes in pillow basalt due to sea-floor weathering, *J. Geophys. Res.*, *77*, 6459–6469, doi:10.1029/JB077i032p06459.

Morris, T. H., D. L. Clark, and S. M. Blasco (1985), Sediments of the Lomonosov Ridge and Makarov Basin: A Pleistocene stratigraphy for the North Pole, *Geol. Soc. Am. Bull.*, *96*, 901–910, doi:10.1130/0016-7606(1985)96<901:SOTLRA>2.0.CO;2.

Moskowitz, B. M. (1980), Theoretical grain size limits for single-domain, pseudo-single-domain and multi-domain behavior in titanomagnetite (x = 0.6) as a function of low-temperature oxidation, *Earth Planet. Sci. Lett.*, *47*, 285–293, doi:10.1016/0012-821X(80)90045-X.

Nishitani, T., and M. Kono (1983), Curie temperature and lattice constant of oxidized titanomagnetite, *Geophys. J. R. Astron. Soc.*, *74*, 585–600.

Nowaczyk, N. R., and M. Baumann (1992), Combined high-resolution magnetostratigraphy and nannofossil biostratigraphy for late Quaternary Arctic Ocean sediments, *Deep Sea Res., Part A*, *39*, S567–S601, doi:10.1016/S0198-0149(06)80021-X.

Nowaczyk, N. R., T. W. Frederichs, H. Kassens, N. Nørgaard-Pedersen, R. F. Spielhagen, R. Stein, and D. Weiel (2001), Sedimentation rates in the Makarov Basin, central Arctic Ocean: A paleomagnetic and rock magnetic approach, *Paleoceanography*, *16*, 368–389, doi:10.1029/2000PA000521.

O'Regan, M., J. King, J. Backman, M. Jakobsson, H. Pälike, K. Moran, C. Heil, T. Sakamoto, T. M. Cronin, and R. W. Jordan (2008), Constraints on the Pleistocene chronology of sediments from the Lomonosov Ridge, *Paleoceanography*, *23*, PA1S19, doi:10.1029/2007PA001551.

O'Reilly, W. (1983), The identification of titanomaghemites: Model mechanisms for the maghemitization and inversion processes and their magnetic consequences, *Phys. Earth Planet. Inter.*, *31*, 65–76, doi:10.1016/0031-9201(83)90067-5.

O'Reilly, W., and S. K. Banerjee (1966), Oxidation of titanomagnetites and self-reversal, *Nature*, *211*, 26–28, doi:10.1038/211026a0.

Özdemir, Ö. (1987), Inversion of titanomaghemites, *Phys. Earth Planet. Inter.*, *46*, 184–196, doi:10.1016/0031-9201(87)90181-6.

Özdemir, Ö., and S. K. Banerjee (1981), An experimental study of magnetic viscosity in synthetic monodomain titanomaghemites: Implications for the magnetization of the ocean crust, *J. Geophys. Res.*, *86*, 11,864–11,868, doi:10.1029/JB086iB12p11864.

Özdemir, Ö., and D. J. Dunlop (2010), Hallmarks of maghemitization in low-temperature remanence cycling of partially oxidized magnetite nanoparticles, *J. Geophys. Res.*, doi:10.1029/2009JB006756, in press.

Özdemir, Ö., and W. O'Reilly (1982), Magnetic hysteresis properties of synthetic monodomain titanomaghemites, *Earth Planet. Sci. Lett.*, *57*, 437–447, doi:10.1016/0012-821X(82)90162-5.

Özdemir, Ö., D. J. Dunlop, and B. M. Moskowitz (1993), The effect of oxidation on the Verwey transition in magnetite, *Geophys. Res. Lett.*, *20*, 1671–1674, doi:10.1029/93GL01483.

Petersen, N., and H. Vali (1987), Observation of shrinkage cracks in ocean floor titanomagnetites, *Phys. Earth Planet. Inter.*, *46*, 197–205, doi:10.1016/0031-9201(87)90182-8.

Phillips, R. L., and A. Grantz (1997), Quaternary history of sea ice and paleoclimate in the Amerasia basin, Arctic Ocean, as recorded in the cyclical strata of Northwind ridge, *Geol. Soc. Am. Bull.*, *109*, 1101–1115, doi:10.1130/0016-7606(1997)109<1101:QHOSIA>2.3.CO;2.

Polyak, L., et al. (2009), Quaternary stratigraphy and sedimentation patterns in the western Arctic Ocean, *Global Planet. Change*, *68*, 5–17, doi:10.1016/j.gloplacha.2009.03.014.

Poore, R. Z., R. L. Phillips, and H. J. Rieck (1993), Paleoclimate record for Northwind Ridge, western Arctic Ocean, *Paleoceanography*, *8*, 149–159, doi:10.1029/93PA00146.

Readman, P. W., and W. O'Reilly (1972), Magnetic properties of oxidized (cation deficient) titanomagnetites (Fe, Ti, □)$_3$O$_4$, *J. Geomagn. Geoelectr.*, *24*, 69–90.

Roberts, A. P., and M. Winklhofer (2004), Why are geomagnetic excursions not always recorded in sediments? Constraints from post-depositional remanent magnetization lock-in modeling, *Earth Planet. Sci. Lett.*, *227*, 345–359, doi:10.1016/j.epsl.2004.07.040.

Robertson, D. J., and D. E. France (1994), Discrimination of remanence-carrying minerals in mixtures, using isothermal remanent magnetisation acquisition curves, *Phys. Earth Planet. Inter.*, *82*, 223–234, doi:10.1016/0031-9201(94)90074-4.

Ryall, P. J. C., J. M. Hall, J. Clark, and T. Milligan (1977), Magnetization of oceanic crustal layer 2—Results and thoughts after DSDP Leg[37], *Can. J. Earth Sci.*, *14*, 684–706.

Sejrup, H. P., H. M. Gifford, J. Brigham-Grette, R. Løvlie, and D. Hopkins (1984), Amino acid epimerization implies rapid sedimentation rates in Arctic Ocean cores, *Nature*, *310*, 772–775, doi:10.1038/310772a0.

Spielhagen, R. F., et al. (1997), Arctic Ocean evidence for Late Quaternary initiation of northern Eurasian ice sheets, *Geology*, *25*, 783–786, doi:10.1130/0091-7613(1997)025<0783:AOEFLQ>2.3.CO;2.

Spielhagen, R. F., K. H. Baumann, H. Erlenkeuser, N. R. Nowaczyk, N. Nøorgaard-Pedersen, C. Vogt, and D. Weiel (2004), Arctic Ocean deep-sea record of northern Eurasian ice sheet history, *Quat. Sci. Rev.*, *23*, 1455–1483, doi:10.1016/j.quascirev.2003.12.015.

Steuerwald, B. A., D. L. Clark, and J. A. Andrew (1968), Magnetic stratigraphy and faunal patterns in Arctic Ocean sediments, *Earth Planet. Sci. Lett.*, *5*, 79–85, doi:10.1016/S0012-821X(68)80018-4.

Verhoogen, J. (1956), Ionic ordering and self-reversal in impure magnetites, *J. Geophys. Res.*, *61*, 201–209, doi:10.1029/JZ061i002p00201.

Verhoogen, J. (1962), Oxidation of iron-titanium oxides in igneous rocks, *J. Geol.*, *70*, 168–181, doi:10.1086/626806.

Witte, W. K., and D. V. Kent (1988), Revised magnetostratigraphies confirm low sedimentation rates in Arctic Ocean cores, *Quat. Res.*, *29*, 43–53, doi:10.1016/0033-5894(88)90070-1.

Xu, W., D. R. Peacor, W. A. Dollase, R. Van Der Voo, and R. Beaubeuf (1997), Transformation of titanomagnetite to titanomaghemite: A slow, two-step, oxidation-ordering process in MORB, *Am. Mineral.*, *82*, 1101–1110.